electronics

Article

Active and Reactive Power Optimal Control of Grid-Connected BDFG-Based Wind Turbines Considering Power Loss

Wenna Wang [1], Liangyi Zhang [1], Sheng Hu [2,*], Defu Cai [1], Haiguang Liu [1], Dian Xu [1], Luyu Ma [1] and Jinrui Tang [2]

[1] State Grid Hubei Electric Power Research Institute, Wuhan 430064, China; wangwn1@hb.sgcc.com.cn (W.W.); hbdkydw-2@foxmail.com (L.Z.); caidf4@hb.sgcc.com.cn (D.C.); liuhg22@hb.sgcc.com.cn (H.L.); xudianchn@gmail.com (D.X.); maluyu990725@163.com (L.M.)
[2] School of Automation, Wuhan University of Technology, Wuhan 430074, China; tangjinrui@whut.edu.cn
* Correspondence: hushee@whut.edu.cn

Abstract

Power loss can influence the accuracy of maximum power point tracking (MPPT) control and the efficiency of a brushless doubly fed generator (BDFG)-based wind turbine (BDFGWT). Because power loss is related to both the active power reference and reactive power reference of BDFG, this article proposes active and reactive power optimal control of BDFGWT by considering power loss. Firstly, the mathematical model of BDFGWT, including the wind turbine, BDFG, and back-to-back converter, is established. Then, an active and reactive power optimal control strategy is proposed. In proposed control, the accurate active power reference of power winding (PW) is calculated by considering the active power loss of BDFG; in this way, proposed MPPT control can capture more wind power compared to traditional MPPT control, ignoring the power losses, thus improving the efficiency of BDFGWT. Furthermore, on the basis of the model of BDFG, the relations between reactive power and total active loss are analyzed, and the optimal reactive power control reference to minimize the active power loss is determined. Finally, in order to verify the validity of the proposed control, 2 MW BDFGWT has been constructed, and the proposed method was studied to make a comparison. The results verify that proposed control can maximize the utilization of wind energy, minimize the power loss of the BDFGWT system, and output maximal active power to the power grid.

Keywords: BDFG-based wind turbine (BDFGWT); power loss; optimal control; MPPT

check for updates

Academic Editors: George Kyriakarakos, Georgios Papadakis and Christos-Spyridon Karavas

Received: 30 July 2025
Revised: 26 August 2025
Accepted: 3 September 2025
Published: 5 September 2025

Citation: Wang, W.; Zhang, L.; Hu, S.; Cai, D.; Liu, H.; Xu, D.; Ma, L.; Tang, J. Active and Reactive Power Optimal Control of Grid-Connected BDFG-Based Wind Turbines Considering Power Loss. *Electronics* **2025**, *14*, 3544. https://doi.org/10.3390/electronics14173544

Copyright: © 2025 by the authors. Licensee MDPI, Basel, Switzerland. This article is an open access article distributed under the terms and conditions of the Creative Commons Attribution (CC BY) license (https://creativecommons.org/licenses/by/4.0/).

1. Introduction

In recent years, to solve the problems of the fossil fuel energy crisis and environment and climate change, there have been significant renewable energy developments in many countries. Wind energy is deemed green, clean, inexhaustible, and renewable, and it is receiving increased amounts of attention. For the purpose of making full use of wind energy, a variable-speed–invariable-frequency wind power system has been widely used since it can improve the utilization efficiency of wind energy and realize maximum power point tracking (MPPT) [1–3]. The brushless doubly fed generator (BDFG)-based wind turbine (BDFGWT) is a new type of variable-speed–invariable-frequency wind turbine. In comparison, BDFGWT not only has the same advantages of decoupling power control and a small-sized converter as a conventional slip-ring doubly fed induction generator (DFIG) wind turbine (DFIGWT) but it also has higher reliability, lower maintenance costs, a smaller-sized gearbox, and a stronger low-voltage ride through (LVRT) capability [4–7].

Thus, BDFGWT is regarded as the candidate of conventional DFIGWT and has promising prospects in wind power systems, especially in those where their maintenance is inconvenient, e.g., offshore wind power.

The BDFGWT is capable of running in stand-alone [8–11] or grid-connected modes [4–7]. Figure 1 illustrates the topology of BDFGWT. According to Figure 1, BDFGWT includes a wind turbine, gearbox, BDFG, grid-side converter (GSC) and machine-side converter (MSC), and controllers. In addition, as illustrated, PW, RW, and CW represent power winding, rotor winding, and control winding of BDFG, respectively.

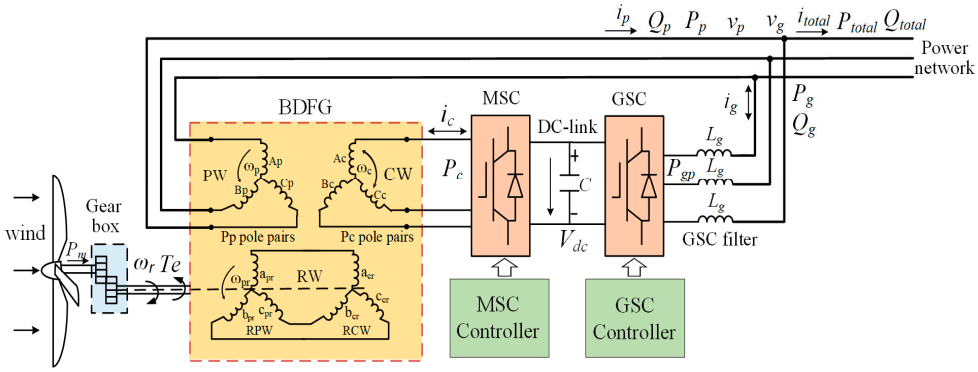


Figure 1. Topology of grid-connected BDFGWT.

Due to the aforementioned advantages, there are many research studies that have focused on BDFGWT. The model and control strategies of BDFG have been well studied in [12–25]. For the purpose of improving the dynamic control property, the vector controls of BDFG were proposed in [13–16]. In [6,7], low-voltage ride through (LVRT) controls under grid fault conditions were studied. Moreover, for the purpose of improving the capability to withstand unbalanced grid voltage, some articles aimed to research BDFGWT under unbalanced grid voltage conditions [17–24]. In addition, because wind energy has the characteristics of volatility and randomicity, for the purpose of improving the efficiency of wind turbines and realizing the economic operation of wind power systems, MPPT control is usually used for wind turbines under rated wind speed. The MPPT control algorithm, based on the power signal feedback for BDFGWT, has been investigated in [6,23–25]; however, the power loss of BDFG is ignored in these MPPT controls. Therefore, the active power reference of PW is not accurate; this causes BDFGWT to not be able to work at its optimal speed and, hence, not being able to output its maximum power. Thus, the efficiency of BDFGWT decreases. Furthermore, besides the active power reference, the reactive power reference of BDFG can also influence power loss; therefore, the efficiency of BDFGWT is also influenced by reactive power reference. Aiming to solve such problems, in this article, active and reactive power optimal control by considering power losses for BDFGWT is proposed. In the proposed control, the accurate active power reference of PW is calculated by considering the power loss of BDFG. In this way, proposed MPPT control can capture more wind power compared to traditional MPPT control, ignoring the power losses; therefore, the efficiency of BDFGWT can be improved. Furthermore, on the basis of BDFG's model, the relations between reactive power and total active loss are analyzed, and the PW optimal reactive power control reference, minimizing the active power loss, is determined. As a result, with proposed control, power loss can be minimized, and the efficiency of BDFGWT can be greatly improved.

The organization of this article is detailed below. First, the mathematical model of BDFGWT, including the wind turbine, BDFG, and back-to-back converter, is established in Section 2. Afterwards, an active and reactive power optimal control strategy is proposed

in Section 3. 2 MW grid-connected BDFGWT is constructed and the proposed method is studied by providing a comparison in Section 4. In Section 5, the conclusions and future work are summarized.

2. Mathematical Model of BDFGWT

2.1. Model of Wind Turbine and MPPT

The output mechanical power of the wind turbine captured from input wind energy is expressed as [1–3,26,27]

$$P_m = \frac{1}{2}\rho\pi R^2 C_P(\lambda,\beta)v^3 \tag{1}$$

In Equation (1), P_m denotes output mechanical power, v denotes wind speed, ρ and R denote the air density and turbine radius, C_p denotes the power coefficient, and β and λ represent pitch angle and the tip–speed ratio, respectively.

The tip–speed ratio λ can be expressed as

$$\lambda = \frac{\omega_m R}{v} \tag{2}$$

In Equation (2), ω_m denotes wind turbine's rotating speed. The power coefficient C_p can be expressed as [1,2]

$$\begin{cases} C_P(\lambda,\beta) = c_1(c_2/\lambda_i - c_3\beta - c_4)e^{-\frac{c_5}{\lambda_i}} + c_6\lambda \\ \frac{1}{\lambda_i} = \frac{1}{\lambda+c_7\beta} - \frac{c_8}{1+\beta^3} \end{cases} \tag{3}$$

where $c_1 = 0.5176$, $c_1 = 116$, $c_3 = 0.4$, $c_4 = 5$, $c_5 = 21$, $c_6 = 0.0068$, $c_7 = 0.08$, $c_8 = 0.035$; λ_i is the intermediate variable.

According to Equation (3), Figure 2 shows the characteristic curve of C_p versus λ and β. As shown, when β is constant (e.g., $\beta = 15°$, $\beta = 10°$, $\beta = 5°$), C_p is only related to λ, and there exists a maximal power coefficient C_{pmax} (e.g., C_{pmax1}, C_{pmax2}, C_{pmax3}), where λ is equal to the optimal tip–speed ratio λ_{opt} (e.g., λ_{opt1}, λ_{opt2}, λ_{opt3}). Thus, according to Equation (2), under a certain pitch angle, for the purpose of keeping λ_{opt} and capturing the maximal wind energy, the rotating speed ω_m should change with the wind speed v.

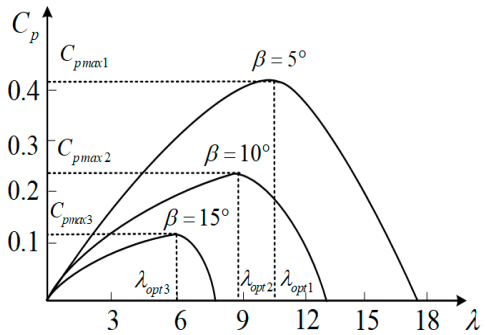


Figure 2. Characteristic curve of C_p versus λ and β.

According to Equations (1) and (3), when β is constant, the relationship between P_m and ω_m can be deduced, and Figure 3 shows their characteristic curve under different wind speeds. As shown, under certain wind speeds (e.g., v_{w1}, v_{w2}, v_{w3}), the outputted mechanical power of the wind turbine changes with rotating speed, and the maximal power P_{mopt} (e.g., P_1, P_2, P_3) is outputted under optimal rotating speed (e.g., ω_1, ω_2, ω_3), namely

λ_{opt} and C_{pmax}. Thus, when the wind turbine works at λ_{opt} and Equation (2) is substituted into Equation (1), the outputted maximal mechanical power P_{mopt} is deduced as [1,3]

$$P_{mopt} = \frac{0.5\rho\pi R^5 C_{pmax}}{\lambda_{opt}^3}\omega_m^3 = k_{opt}\omega_m^3 \tag{4}$$

where $k_{opt} = 0.5\rho\pi R^5 C_{pmax}/\lambda_{opt}^3$.

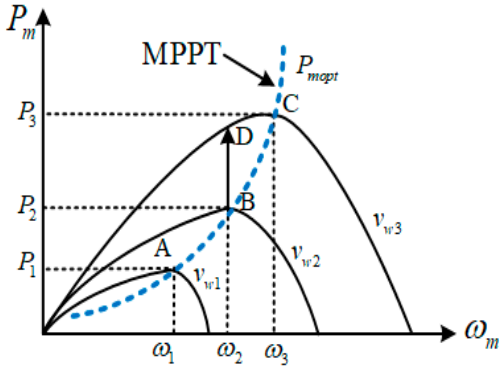


Figure 3. Power curve of ω_m versus v_w.

Based on Equation (4), the maximal power curve is plotted in Figure 3. According to Figure 3, when wind speed varies, in order to capture maximal wind energy, the outputted power of the generator needs to be controlled to track the maximal power curve; this way, the mechanical rotating speed can operate at optimal rotating speed in a stable state. This is known as MPPT control.

2.2. Mathematical Model of BDFG (MSC)

The mathematical model of BDFG under the unified PW flux rotating reference frame is represented as [12,15,16,19,21–23,28]

$$u_p = r_p i_p + \frac{d\varphi_p}{dt} + j\omega_p\varphi_p \tag{5}$$

$$u_c = r_c i_c + \frac{d\varphi_c}{dt} + j\omega_c\varphi_c \tag{6}$$

$$u_r = r_r i_r + \frac{d\varphi_r}{dt} + j\omega_{pr}\varphi_r \tag{7}$$

$$\varphi_p = L_p i_p + L_{pr} i_r \tag{8}$$

$$\varphi_c = L_c i_c - L_{cr} i_r \tag{9}$$

$$\varphi_r = L_r i_r + L_{pr} i_p - L_{cr} i_c \tag{10}$$

where u_p, u_c, u_r, i_p, i_c, i_r, φ_p, φ_c, and φ_r denote voltage, current, and flux spatial vectors of PW, CW, and RW under the PW flux reference frame; $\omega_{pr} = \omega_p - p_p\omega_r$, $\omega_c = \omega_p - (p_p + p_c)\omega_r$, p_p, and p_c represent the pole pairs of PW and CW; ω_p, ω_{pr}, ω_c, and ω_r denote the rotating speed of PW flux, RPW flux, CW flux, and rotor; r_p, r_c, r_r, L_p, L_c, and L_r represent resistances and self-inductances of PW, CW, and RW; L_{pr} and L_{cr} represent mutual inductances between PW and RW and CW and RW; and $u_r = 0$, where subscripts p, c, and r represent PW, CW, and RW.

The RW current is calculated using Equation (8)

$$i_r = \frac{\varphi_p}{L_{pr}} - \frac{L_p}{L_{pr}} i_p \tag{11}$$

Substituting Equation (11) into Equations (9) and (10) yields

$$\varphi_r = \frac{L_r}{L_{pr}}\varphi_p - L_M i_p - L_{cr} i_c \tag{12}$$

$$\varphi_c = L_c i_c - \frac{L_{cr}}{L_{pr}}\varphi_p + \frac{L_{cr}L_p}{L_{pr}} i_p \tag{13}$$

Using Equations (11) and (12), Equation (7) becomes

$$r_r\left(\frac{\varphi_p - L_p i_p}{L_{pr}}\right) + \frac{L_r}{L_{pr}}\frac{d\varphi_p}{dt} - L_M\frac{di_p}{dt} - L_{cr}\frac{di_c}{dt} + j\omega_{pr}\left(\frac{L_r}{L_{pr}}\varphi_p - L_M i_p - L_{cr} i_c\right) = 0 \tag{14}$$

where $L_M = (L_r L_p / L_{pr}) - L_{pr}$.

Using Equations (13) and (14), the CW voltage in Equation (6) can be deduced as

$$u_c = r_c i_c + \sigma L_c \frac{di_c}{dt} + K_c \tag{15}$$

In (15), σ is the leakage factor and $\sigma = 1 - L^2{}_{cr}L_p/(L_{pr}L_M L_c)$ and K_c are the total cross-couplings and disturbances, represented as

$$K_c = \left(j\omega_c L_c - j\frac{\omega_{pr}L_{cr}^2 L_p}{L_{pr}L_M}\right)i_c + \left(j\frac{\omega_c L_{cr}L_p - \omega_{pr}L_{cr}L_p}{L_{pr}} - \frac{r_r L_p^2 L_{cr}}{L_{pr}^2 L_M}\right)i_p + \left(-j\frac{\omega_c L_{cr}}{L_{pr}} + \frac{r_r L_p L_{cr}}{L_{pr}^2 L_M} + j\frac{\omega_{pr}L_{cr}L_p L_r}{L_{pr}^2 L_M}\right)\psi_p \tag{16}$$

Moreover, according to Equation (14), with r_r ignored, the CW current in the steady state is represented as

$$i_c = \frac{L_r}{L_{pr}L_{cr}}\varphi_p - \frac{L_M}{L_{cr}} i_p \tag{17}$$

The apparent power of PW can be represented as [18–20]

$$S_p = P_p + jQ_p = \frac{3}{2}u_p\hat{i}_p \tag{18}$$

In Equation (18), $\hat{i}_p$ is the conjugate value of i_p and S_p, P_p, and Q_p are the apparent, active, and reactive powers of PW, calculated through adopting PW flux orientation and using the dq components of voltage and current vectors and Equation (17), as follows:

$$P_p = \frac{3}{2}(u_{pd}i_{pd} + u_{pq}i_{pq}) = \frac{3}{2}u_{pq}i_{pq} = -\frac{3}{2}\frac{L_{cr}}{L_M}u_{pq}i_{cq} \tag{19}$$

$$Q_p = \frac{3}{2}(u_{pq}i_{pd} - u_{pd}i_{pq}) = \frac{3}{2}u_{pq}i_{pd} = -\frac{3}{2}\frac{L_{cr}}{L_M}\left(i_{cd} - \frac{L_r}{L_{pr}L_{cr}}\psi_{pd}\right) \tag{20}$$

Therefore, as indicated by Equations (19) and (20), the PW active and reactive powers are capable of being controlled by q and d components of the CW current, respectively.

2.3. Mathematical Model of GSC

The mathematical model of GSC in the dq rotating reference frame is given by [22,23]

$$u_g = r_g i_g + L_g\frac{di_g}{dt} + j\omega_p i_g + u_{gp} \tag{21}$$

$$C\frac{dV_{dc}}{dt}\cdot V_{dc} = P_{gp} - P_c \tag{22}$$

In Equations (21) and (22), r_g and L_g are the resistance and inductance of GSC's filter; C and V_{dc} are the capacitance and voltage of DC bus; and u_g, u_{gp}, P_{gp}, and P_c denote the grid voltage, GSC pole voltage, GSC pole, and CW active powers, as illustrated in Figure 1.

The output GSC's active and reactive powers are given by [19,20]

$$P_g = \frac{3}{2}(u_{gd}i_{gd} + u_{gq}i_{gq}) \tag{23}$$

$$Q_p = \frac{3}{2}(u_{gq}i_{gd} - u_{gd}i_{gq}) \tag{24}$$

3. Proposed Active and Reactive Power Optimal Control of BDFGWT

The control for BDFGWT consists of the MSC(BDFG) controller and GSC controller. For the MSC(BDFG) controller, the control targets are usually the active and reactive powers exchanged with the power grid, and the control model for the MSC controller has been derived from Equations (15), (16), (19), and (20). For the GSC controller, the control targets include keeping the DC-link voltage as constant and achieving sinusoidal current input and unity power factor control, and the control model for the GSC controller has been derived from Equations (21)–(24). Thus, based on the control targets and the derived models of MSC(BDFG) and GSC, the proposed optimal control strategy of the grid-connected BDFGWT system is shown in Figure 4. As can be seen, the GSC controller consists of the DC-link voltage outer loop plus the inner loop of the GSC current to achieve GSC's control target; at the same time, in the MSC controller, the active and reactive powers of PW can be regulated by the MSC current. As analyzed in Section 2.1, in order to capture maximal wind energy, the PW active power reference is computed according to MPPT control, but the active power loss of BDFG is usually ignored during computation; therefore, the PW active power control reference is actually not accurate. This causes BDFGWT to not be able to follow its optimal speed and hence not capture the maximum amount of power. Furthermore, the power loss of BDFG is also related to the PW reactive power reference. Thus, in order to capture maximal wind power and minimize power loss, in proposed control, the accurate active power control reference of PW is calculated by considering BDFG's active power loss and the optimal control reference of PW reactive power; this way, the power loss of BDFGWT is determined. The optimal control references of PW active and reactive powers can be calculated as follows:

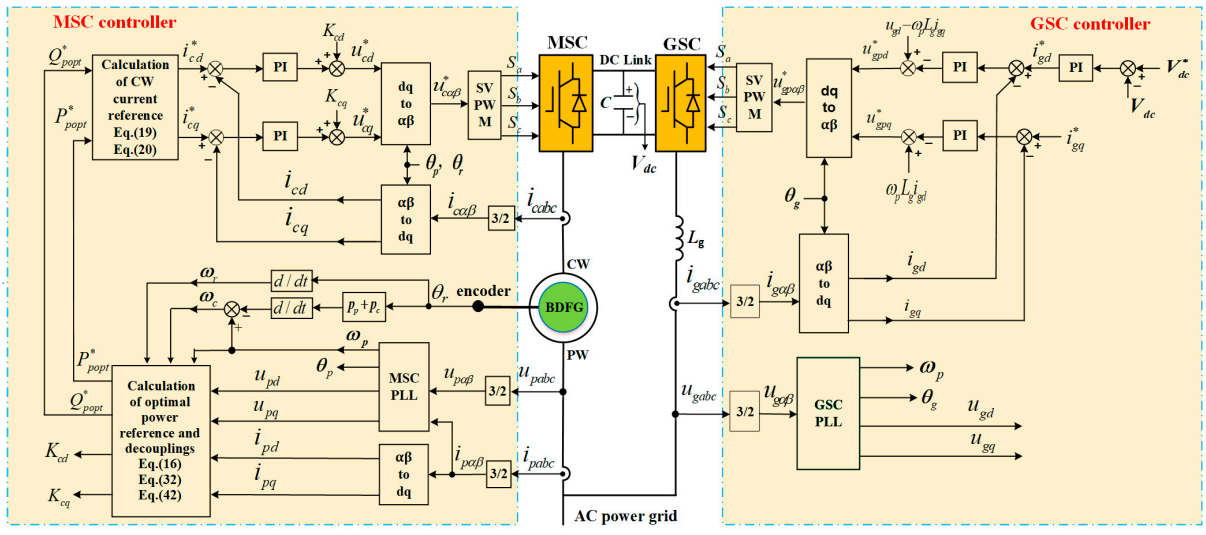


Figure 4. Proposed active and reactive power optimal control strategy for BDFGWT.

3.1. Proposed MPPT Control and PW Active Power Control Reference Calculation

Figure 5 shows the active power flow of BDFG. In Figure 5, P_m, P_{mp}, and P_{mc} represent the total input mechanical power of BDFG, the mechanical power related to PW, and the mechanical power related to CW; P_{mep}, P_{er}, p'_p, and P_p represent PW electromagnetic power, slip power related to PW, copper loss of PW, and output active power of PW; P_{mec}, P_{ec}, p'_r, p'_c, and P_c represent CW electromagnetic power, slip power related to CW, copper loss of RW, copper loss of CW, and output active power of CW; and s_p and s_c represent the slip rates of PW and CW, respectively. According to Figure 5, the relationship of BDFG's active power is represented as

$$P_p = P_{mep} - p'_p \tag{25}$$

$$P_{mep} : P_{mp} : P_{er} = 1 : (1 - s'_p) : s'_p \tag{26}$$

$$P_{er} = P_{mec} - p'_r \tag{27}$$

$$P_{mec} : P_{mc} : P_{ec} = 1 : (1 - s'_c) : s'_c \tag{28}$$

$$P_{ec} = P_c - p'_c \tag{29}$$

$$P_m = P_{mp} + P_{mc} \tag{30}$$

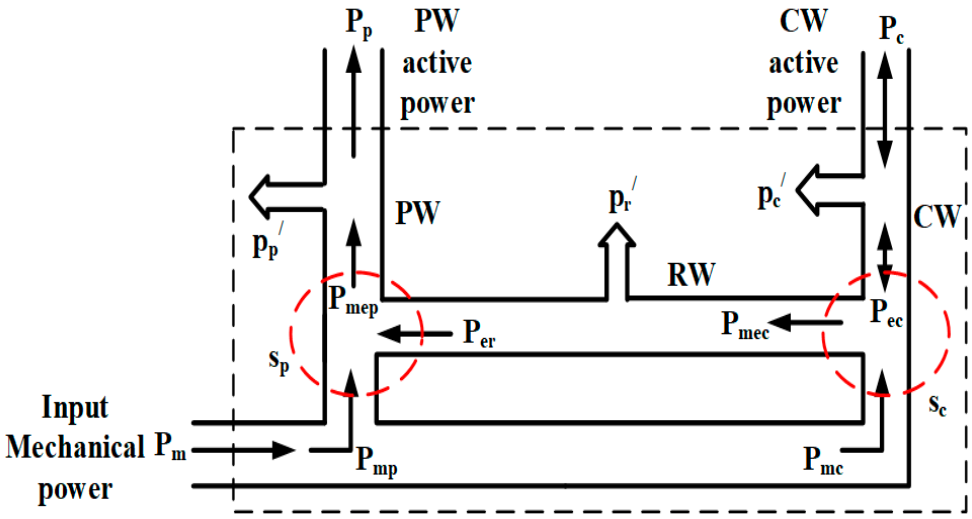


Figure 5. Active power flow of BDFG.

By combining Equations (25)–(27), and (30) and not ignoring the copper loss of PW and RW, the PW active power is derived as

$$P_p = \frac{P_m}{1 - s'_p s'_c} + \frac{s'_c p'_r}{1 - s'_p s'_c} - p'_p \tag{31}$$

In order to realize MPPT control, substituting Equation (4) into Equation (31), the accurate control reference of PW active power considering the copper loss can be calculated as

$$P^*_{popt} = \frac{k_{opt}\omega_m^3}{1 - s'_p s'_c} + \frac{s'_c p'_r}{1 - s'_p s'_c} - p'_p \tag{32}$$

In Equation (32), if the copper losses p'_p and p'_r are ignored, then the control reference of PW active power is calculated as

$$P^*_{papprox} \approx \frac{k_{opt}\omega_m^3}{1 - s_p' s_c'} \tag{33}$$

It is worth noting that Equation (33) is usually used to approximately calculate the PW active power reference in traditional MPPT control; however, since the copper losses p_p' and p_r' are ignored, the PW active power reference is not accurate, and this causes traditional MPPT control to not be able to capture maximal wind energy. In contrast, in proposed MPPT control, the accurate PW active power reference is calculated by using Equation (32), where the copper losses are all considered; therefore, MPPT control can be realized as expected.

3.2. Optimal Reactive Power Control Reference Calculation

Apart from the MPPT control algorithm, the efficiency of the wind energy conversion is also influenced by the power loss of BDFG. The power loss is related to both active and reactive power control references. Thus, for the purpose of reducing the power loss and improving the efficiency of BDFGWT, the reactive power control reference also needs to be optimized. The total power losses of BDFG mainly include PW copper loss p_p', RW copper loss p_r', and CW loss p_c', which can be expressed as

$$p_{lossT} = p_p' + p_r' + p_c' \tag{34}$$

In Equation (34), P_{lossT} represents the total power losses of BDFG, and the copper losses of PW, RW, and CW are expressed as

$$p_p' = \frac{3}{2}|i_p|^2 r_p = \frac{3}{2}(i_{pd}^2 + i_{pq}^2) r_p \tag{35}$$

$$p_r' = \frac{3}{2}|i_r|^2 r_r = \frac{3}{2}(i_{rd}^2 + i_{rq}^2) r_r \tag{36}$$

$$p_c' = \frac{3}{2}|i_c|^2 r_c = \frac{3}{2}(i_{cd}^2 + i_{cq}^2) r_c \tag{37}$$

By using the PW flux-oriented method, i.e., $\varphi_{pd} = \varphi_p$, $\varphi_{pq} = 0$, and substituting Equation (11) into Equations (36) and (17) into Equation (37), the copper losses of RW and CW can be calculated as

$$p_r' = \frac{3}{2}\left[\left(\frac{\varphi_{pd} - L_{pr} i_{pd}}{L_{pr}}\right)^2 + \frac{L_p^2 i_{pq}^2}{L_{pr}^2}\right] r_r \tag{38}$$

$$p_r' = \frac{3}{2}\left[\left(\frac{L_r \varphi_{pd} - L_{pr} L_M i_{pd}}{L_{pr} L_{cr}}\right)^2 + \frac{L_M^2 i_{pq}^2}{L_{cr}^2}\right] r_c \tag{39}$$

Substituting Equations (35), (38), and (39) into Equation (34) yields

$$\begin{aligned} p_{lossT} &= \tfrac{3}{2}\left[\left(r_p + \frac{L_p^2 r_r}{L_{pr}^2} + \frac{L_M^2 r_c}{L_{cr}^2}\right) i_{pd}^2 - \left(\frac{2L_p \varphi_{pd} r_r}{L_{pr}^2} + \frac{2L_r L_M \varphi_{pd} r_c}{L_{cr}^2 L_{pr}}\right) i_{pd} + \left(\frac{\varphi_{pd}^2 r_r}{L_{pr}^2} + \frac{L_r^2 \varphi_{pd}^2 r_c}{L_{pr}^2 L_{cr}^2}\right) + \left(r_p + \frac{L_p^2 r_r}{L_{pr}^2} + \frac{L_M^2 r_c}{L_{cr}^2}\right) i_{pq}^2\right] \\ &= a i_{pd}^2 + b i_{pd} + c \end{aligned} \tag{40}$$

Equation (40) can be deemed as quadratic polynomial with variable i_{pd}; therefore, the minimum value of the total power losses P_{lossT} occurs when i_{pd} satisfies

$$i_{pd} = -\frac{b}{2a} = \frac{L_p \varphi_{pd} L_{cr}^2 r_r + L_r L_M L_{pr} \varphi_{pd} r_c}{r_p L_{pr}^2 L_{cr}^2 + L_p^2 L_{cr}^2 r_r + L_{pr}^2 L_M^2 r_c} \tag{41}$$

Thus, by combining Equations (20) and (41), the optimal reactive power control reference to minimize the power loss of BDFG can be derived as

$$Q_{popt} = \frac{1.5\left(L_p\varphi_{pd}L_{cr}^2 r_r u_{pq} + L_r L_M L_{pr}\varphi_{pd} r_c u_{pq}\right)}{r_p L_{pr}^2 L_{cr}^2 + L_p^2 L_{cr}^2 r_r + L_{pr}^2 L_M^2 r_c} \tag{42}$$

In the proposed control shown in Figure 4, Equation (42) is used to calculate the optimal reactive power control reference; hence, the power loss is minimal and the efficiency of wind energy conversion can be greatly improved.

4. Simulation Verification

For the purpose of verifying the validity of the proposed power optimal control, the 2 MW BDFGWT system was constructed and studied using Matlab 7.8.0(R2009a)-Simulink. The parameters of BDFGWT are listed in Tables A1 and A2 in Appendix A, respectively. In all cases, at the GSC side, the control reference of DC-link voltage V_{dc}^* is 1200 V, and the GSC reactive power reference Q_g^* is 0 MVar (i.e., $i^*_{gq} = 0$).

Figure 6 shows the results where the traditional MPPT control ignoring copper losses and proposed MPPT control considering copper losses are compared. In such case, wind speed is initially set as 5 m/s, and the step is changed from 5 m/s to 10 m/s at 1 s; for the MSC controller, the PW active power reference P_p^* is calculated using Equations (32) and (33) in Section 3.1, respectively, while the PW reactive power reference Q_p^* is set as 0 MVar. As can be seen from Figure 6a,d due to less wind speed before 1 s, the output mechanical powers of wind turbine P_{m} by traditional MPPT control and proposed MPPT control are also smaller, and they are almost both equal to 0.17p.u. Moreover, it is also can be seen from Figure 6b,c,g that power coefficients, rotor speeds, and total output active power into the power grid using traditional MPPT control and proposed MPPT control are almost equal before 1 s; this is due to the fact that the copper losses are small before 1 s and hence its impact on traditional and proposed MPPT controls can be ignored. However, when wind speed steps up from 5 m/s to 10 m/s at 1 s and the whole BDFGWT system reaches the new steady state after 1.6 s, as shown in Figure 6b, the power coefficient is equal to 0.48 under proposed MPPT control and larger than that under traditional MPPT control, which is approximately 0.46. Thus, the wind turbine can capture more wind energy by using proposed MPPT control than when using traditional MPPT control; this is also verified by the results in Figure 6c,d,g, where rotor speeds, P_m, and P_{total} under proposed MPPT control are larger than those under traditional MPPT control. As analyzed previously in theory, the calculation of PW active power control reference in the proposed MPPT control considers the copper losses to be much more accurate than those of traditional MPPT control, and Figure 6e shows their differences. Moreover, according to Figure 6c,f, when the rotor speeds vary from sub-synchronous state to super-synchronous state, GSC active power changes from negative to positive, which means that GSC absorbs slip power before 1 s and then changes into delivering slip power. In addition, as can be observed from Figure 6h, DC-link voltage and PW reactive power track with their control references very well and ensure that the control targets are set as expected.

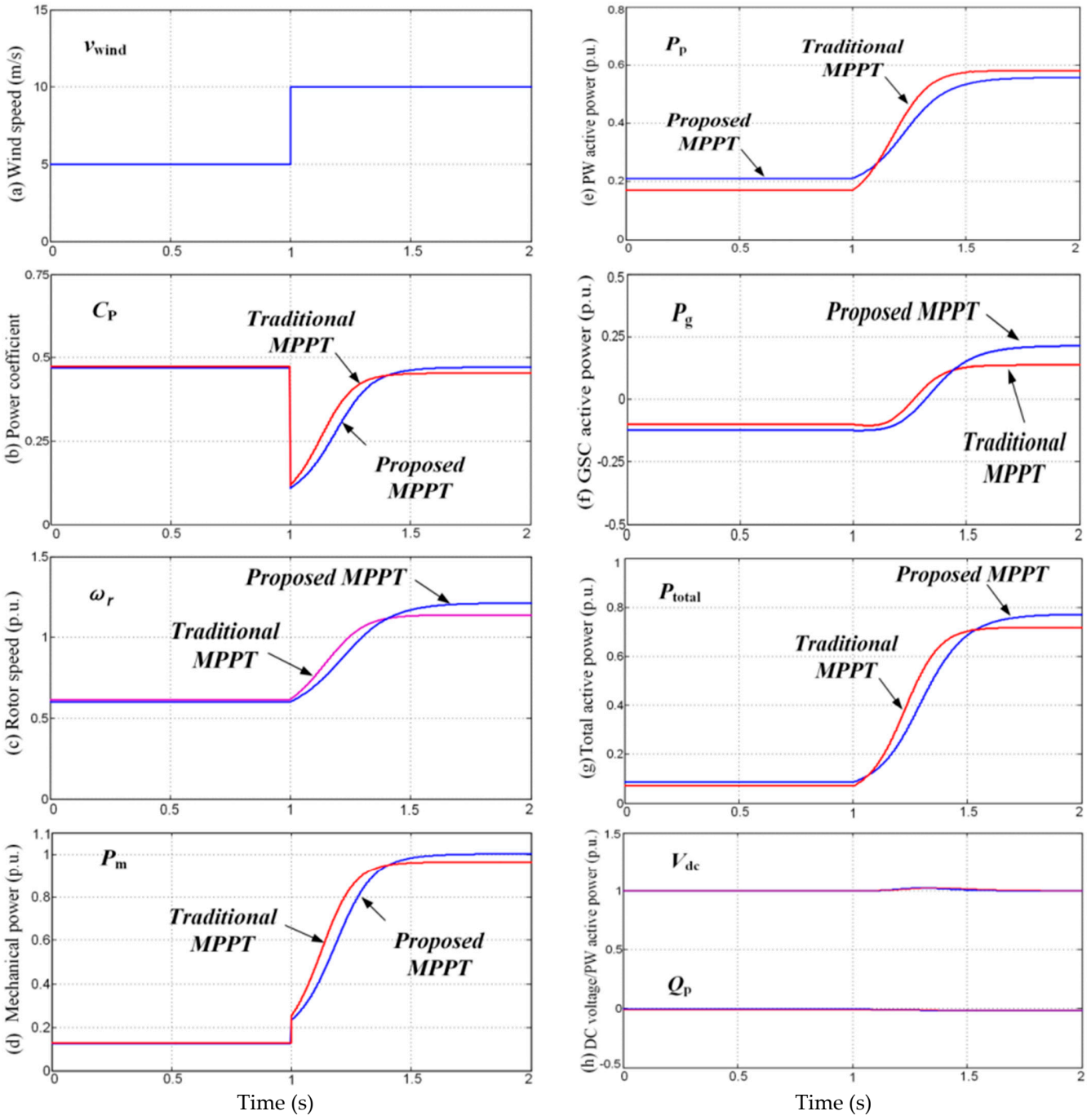


Figure 6. Waveforms of traditional MPPT control and proposed MPPT control. (**a**) Wind speed (m/s). (**b**) Power coefficient. (**c**) Rotor speed (p.u.). (**d**) Output mechanical power of wind turbine (p.u.). (**e**) PW active power (p.u.). (**f**) GSC active power (p.u.). (**g**) Total output active power into power grid (p.u.). (**h**) DC-link voltage and PW reactive powers (p.u.).

Figure 7 shows the results of BDFGWT under varying PW reactive powers. Figure 7A shows the waveforms under sub-synchronous state with a rotor speed of 0.7p.u., and Figure 7B shows the waveforms under super-synchronous state with a rotor speed of 1.3p.u. For MSC controller, P_p^* is set to 0.5p.u. all the time, whereas Q_p^* is initially set as -0.75p.u. (capitative reactive power) and then ramps up from -0.75p.u. at 0.5 s to 0.3p.u. (inductive reactive power) at 1.55 s. It can be seen in Figure 7(Ae,Af) that when the PW reactive power control reference changes from -0.75p.u. to 0.3p.u., the total copper losses initially decrease, reach their minimum value at 1 s, and then increase. The same also occurs in Figure 7(Be,Bf) under

super-synchronous state. Furthermore, it can also be observed that the minimum value of copper losses occurs only when Q_p^* is equal to its optimal value, i.e., $Q_{popt} = -0.25$p.u. Simultaneously, Q_{popt}^* can also be calculated by Equation (42), and it is almost equal to the simulation result, namely $Q_{popt} = -0.25$p.u.; therefore, the results agree well with the theoretical analysis in Section 3.2. In addition, as shown in Figure 7(Ad,Bd), the total output current of BDFGWT under super-synchronous state is larger than that under sub-synchronous state; this is because both PW and GSC output active currents under super-synchronous state while GSC absorbs active currents under sub-synchronous state.

We performed a further study on proposed control, where Q_p^* is set as $Q_{popt}^* = -0.25$p.u., and 0p.u has been investigated; Figure 8 shows the comparison results. Wind speed was initially set as 5 m/s and changed from 5 m/s to 10 m/s at 1 s; for the MSC controller, the PW active power control reference is given by the proposed accurate MPPT algorithm that is expressed as Equation (32) in Section 3.1, while Q_p^* is set as $Q_{popt}^* = -0.25$p.u and 0p.u., respectively. It can be seen in Figure 8a,b that the output mechanical powers and power coefficients of the wind turbine under $Q_p^* = Q_{popt}^* = -0.25$p.u. and $Q_p^* = 0$p.u. are close at steady state; this is owed to the proposed accurate MPPT algorithm. However, it can be clearly observed from Figure 8e,h that the total copper losses under $Q_{popt}^* = -0.25$p.u. are less than those under $Q_p^* = 0$p.u. at steady state, and this causes the total output active power of BDFGWT under $Q_{popt}^* = -0.25$p.u. to be larger than that under $Q_p^* = 0$p.u., which can also be observed from Figure 8g. As a result, the power loss of the BDFGWT system is minimized and maximal active power is outputted to the power grid using proposed optimal control. In addition, because the copper losses under $Q_{popt}^* = -0.25$p.u. and 0p.u. are different, PW active power and GSC active power are also affected, which are shown in Figure 8d,f. Thus, the results agree with the theoretical analysis and verify the superiority of proposed active and reactive power optimal control again.

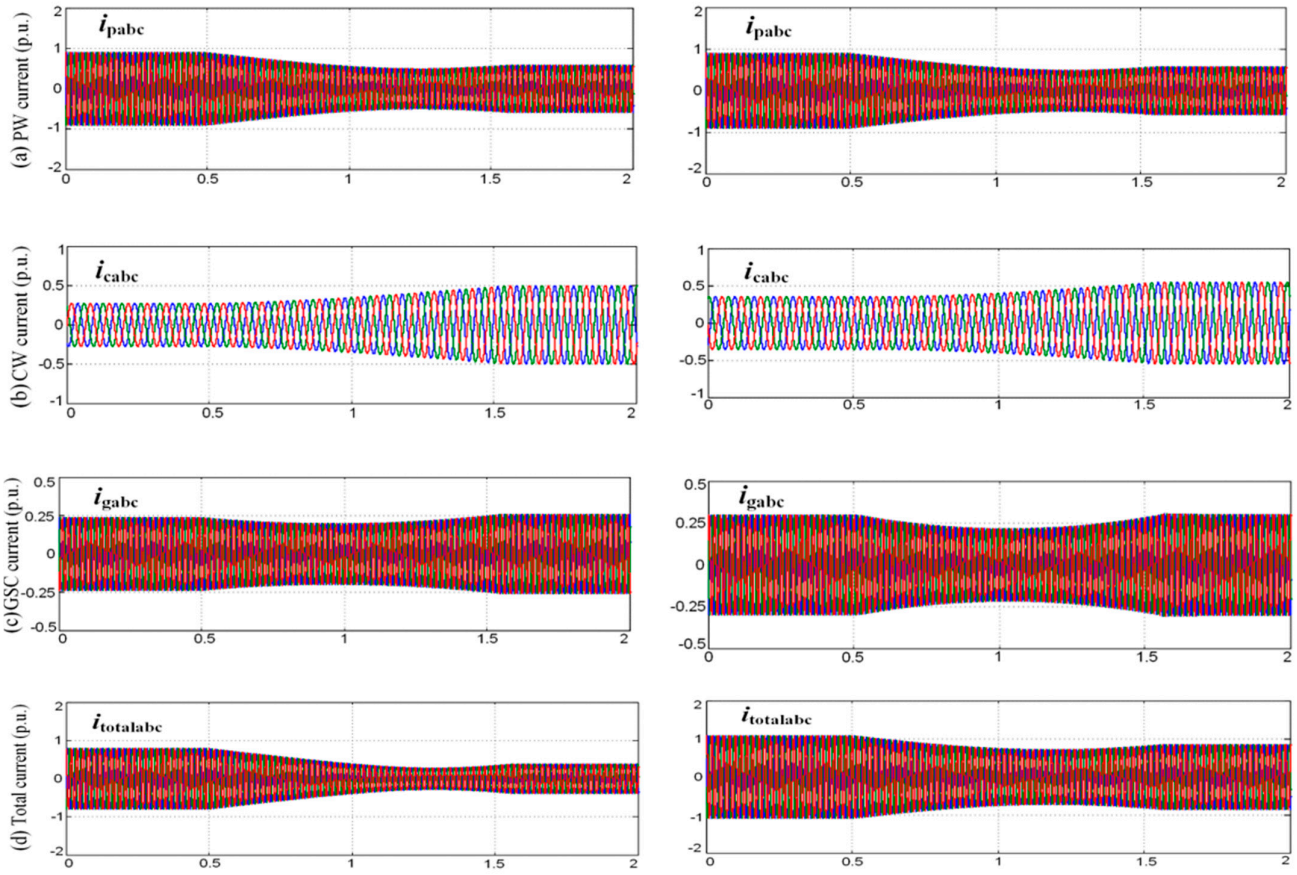
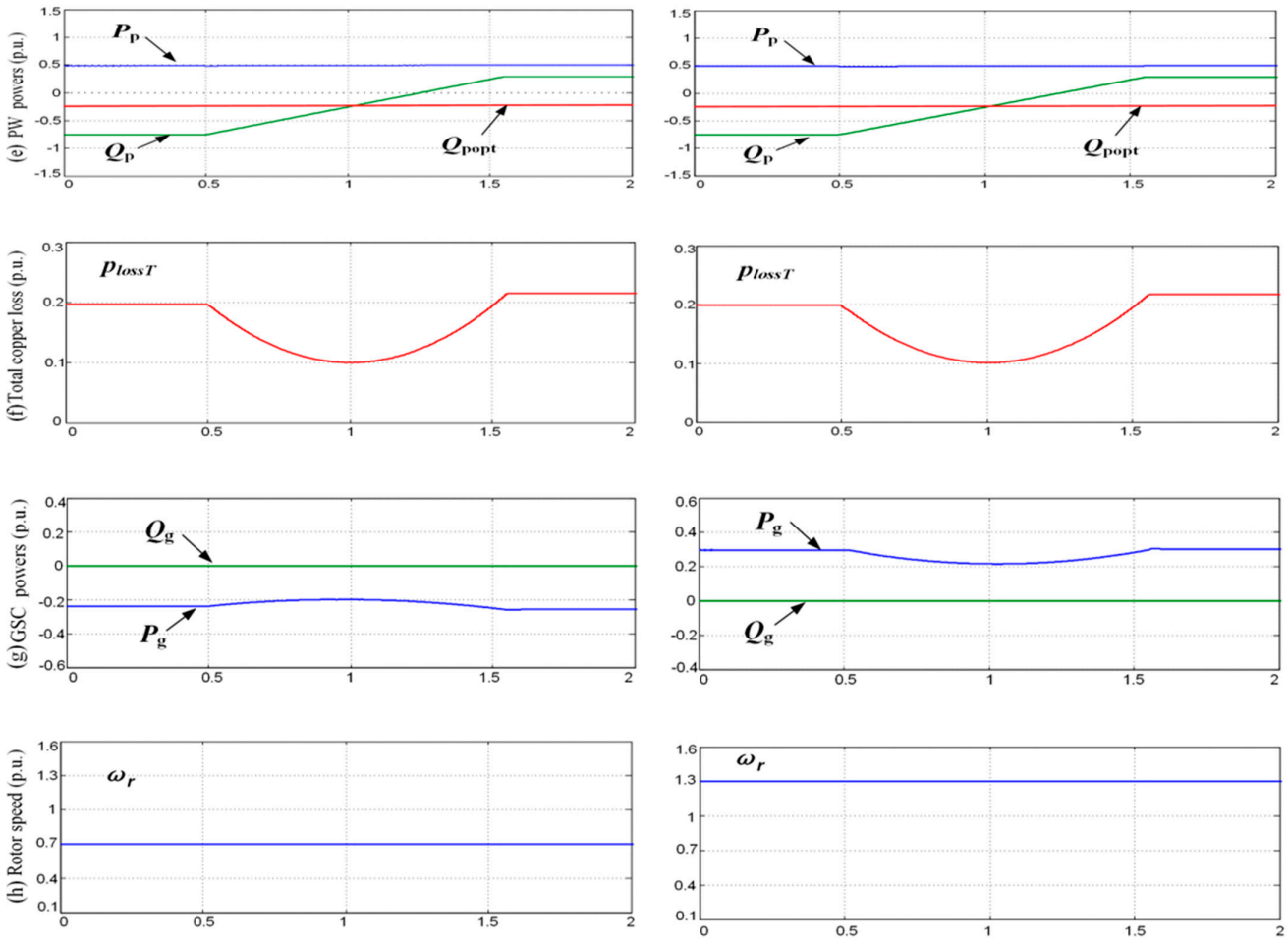


Figure 7. *Cont.*



(**A**) (**B**)

Figure 7. Waveforms of BDFGWT under varying PW reactive power. (**a**) PW currents (p.u.). (**b**) CW currents (p.u.). (**c**) GSC currents (p.u.). (**d**) Total output currents of BDFGWT (p.u.). (**e**) PW active power, reactive power, and optimal reactive power (p.u.). (**f**) Total copper loss (p.u.). (**g**) GSC active and reactive powers (p.u.). (**h**) Rotor speed (p.u.). (**A**) Sub-synchronous state (ω_r = 0.7p.u.). (**B**) Super-synchronous state (ω_r = 1.3p.u.).

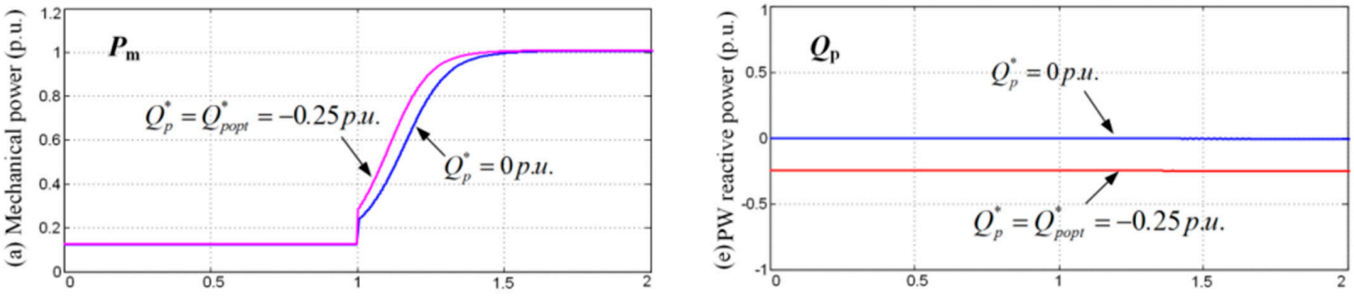


Figure 8. *Cont.*

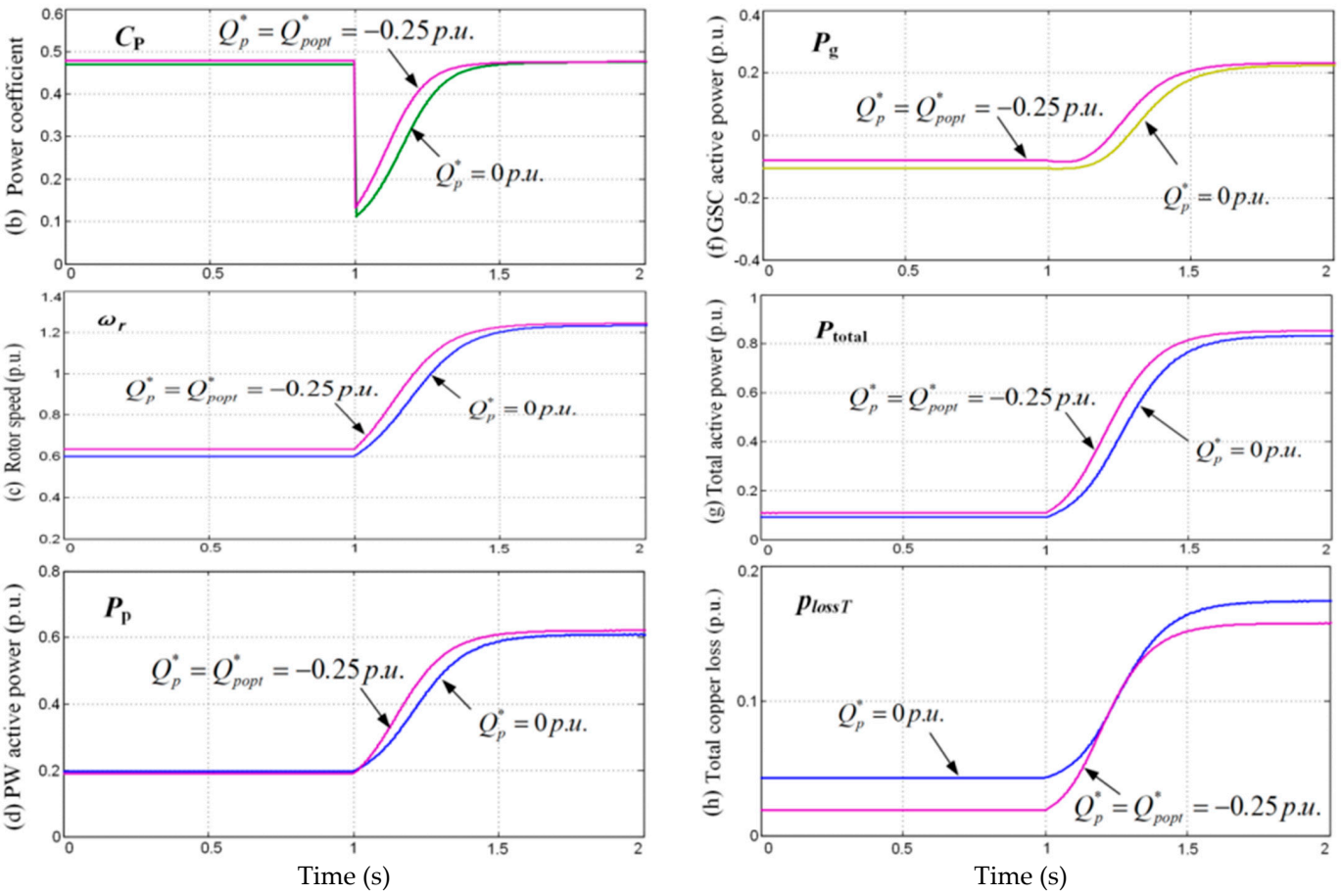


Figure 8. Waveforms of proposed control under $Q_p^* = Q_{popt}^* = -0.25$p.u. and $Q_p^* = 0$p.u. (**a**) Output mechanical power of wind turbine (p.u.). (**b**) Power coefficient. (**c**) Rotor speed (p.u.). (**d**) PW active power (p.u.). (**e**) PW reactive power (p.u.). (**f**) GSC active power (p.u.). (**g**) Total output active power into power grid (p.u.). (**h**) Total copper loss (p.u.).

5. Conclusions

For the purpose of improving the efficiency of wind energy conversion and realizing its economic operation, this article proposes active and reactive power optimal control of the BDFGWT system by considering power loss. On the basis of the mathematical model of the BDFGWT system, including the wind turbine, BDFG, and back-to-back converter, an active and reactive power optimal control strategy is proposed. The accurate active power reference of PW is calculated by considering the active power loss of BDFG; in this way, the proposed MPPT control can capture more wind power compared to traditional MPPT control, ignoring the power losses, thus improving the efficiency of BDFGWT. Furthermore, on the basis of BDFG's model, the relations between reactive power and total active loss are analyzed, and then the optimal reactive power control reference to minimize the active power loss is determined. In order to verify the validity of the proposed control, 2 MW BDFGWT was constructed, and the proposed control was studied in comparison. The results verify that the proposed control is capable of realizing maximal wind energy capture, minimizing the power loss of the BDFGWT system, and outputting maximal active power to the power grid. As a result, the efficiency and economy of the BDFGWT system can be improved using proposed control.

In future work, the efficiency and economic operation of the wind farm installed using the BDFGWT system will be studied.

Author Contributions: Conceptualization, W.W. and S.H.; methodology, W.W. and S.H.; validation, L.Z. and S.H.; formal analysis, D.X. and L.M.; investigation, H.L.; writing—original draft preparation, S.H.; writing—review and editing, S.H.; supervision, D.C. and J.T.; project administration, D.C. and J.T. All authors have read and agreed to the published version of the manuscript.

Funding: This work was supported by the Guideline Project of State Grid Corporation of China [grant numbers 5100-202199536A-0-5-ZN].

Data Availability Statement: The data presented in this study are available in this article.

Conflicts of Interest: Authors Wenna Wang, Liangyi Zhang, Defu Cai, Haiguang Liu, Dian Xu, and Luyu Ma were employed by the company State Grid Hubei Electric Power Research Institute. The remaining authors declare that this research was conducted in the absence of any commercial or financial relationships that could be construed as potential conflicts of interest.

Appendix A

Table A1. Parameters of BDFG and converter.

Parameters	Values
Rated power (MW)	2 MW
Rated voltage (V)	690 V
Rated frequency (Hz)	50 Hz
r_p, r_c, r_r (Ω)	0.0036, 0.0072, 0.3965
L_p, L_c, L_r (mH)	3.1000, 6.8890, 19.050
L_{pr}, L_{cr} (mH)	6.6560, 4.8940
Pole pairs (p_p, p_c)	2, 2
r_g (Ω)	3.1000
L_g (mH)	0.18
C (uF)	2000

Table A2. Parameters of wind turbine and gear box.

Parameters	Values
Rated power (MW)	2 MW
Turbine diameter	93.4 m
Cut-in wind speed	3 m/s
Rated wind speed	10.5 m/s
Gear ratio	59
System inertia	60 Kg·m^2
Friction coefficient	0.007

References

1. Kim, K.; Van, T.; Lee, D.; Song, S.; Kim, E. Maximum output power tracking control in variable speed wind turbine systems considering rotor inertial power. *IEEE Trans. Ind. Electron.* **2013**, *60*, 3207–3217. [CrossRef]
2. Murat, K.; Luis, M.; Tariq, K.; Shyam, K. A new hill climbing maximum power tracking control for wind turbines with inertial effect compensation. *IEEE Trans. Ind. Electron.* **2019**, *60*, 8545–8556. [CrossRef]
3. Syahputra, R.; Soesanti, I. Performance improvement for small-scale wind turbine system based on maximum power point tracking control. *Energies* **2019**, *12*, 3938. [CrossRef]
4. Loukianov, A.; Huerta, H. Energy based sliding mode control of brushless double-fed induction generator. *Int. J. Electr. Power Energy Syst.* **2021**, *130*, 107002. [CrossRef]
5. Strous Tim, D.; Polinder, H.; Ferreira, J.A. Brushless doubly-fed induction machines for wind turbines: Developments and research challenges. *IET Electr. Power Appl.* **2017**, *11*, 991–1000. [CrossRef]
6. Gowaid, I.A.; Abdel-Khalik, A.S.; Massoud, A.M.; Ahmed, S. Ride through capability of grid-connected brushless cascade DFIG wind turbines in faulty grid conditions—A comparative study. *IEEE Trans. Sustain. Energy* **2013**, *4*, 1002–1015. [CrossRef]
7. Long, T.; Shao, S.; Abdi, E.; McMahon, R. Asymmetrical low-voltage ride through of brushless doubly fed induction generators for the wind power generation. *IEEE Trans. Energy Convers.* **2013**, *28*, 502–511. [CrossRef]

8. Cheng, M.; Jiang, Y.; Han, P.; Wang, Q. Unbalanced and low-order harmonic voltage mitigation of stand-alone dual-stator brushless doubly fed induction wind generator. *IEEE Trans. Ind. Electron.* **2018**, *65*, 9135–9146. [CrossRef]
9. Xu, W.; Mohammed, O.M.E.; Liu, Y.; Islam, M.D.R. Negative sequence voltage compensating for unbalanced standalone brushless doubly-fed induction generator. *IEEE Trans. Power Electron.* **2020**, *35*, 667–680. [CrossRef]
10. Liu, Y.; Xu, W.; Zhu, J.; Blaabjerg, F. Sensorless control of standalone brushless doubly fed induction generator feeding unbalanced loads in a ship shaft power generation system. *IEEE Trans. Ind. Electron.* **2019**, *66*, 739–749. [CrossRef]
11. Liu, Y.; Xu, W.; Long, T.; Blaabjerg, F. An improved rotor speed observer for standalone brushless doubly-fed induction generator under unbalanced and nonlinear Loads. *IEEE Trans. Power Electron.* **2020**, *35*, 775–788. [CrossRef]
12. Han, P.; Cheng, M.; Wei, X.; Li, N. Modeling and performance analysis of a dual-stator brushless doubly fed induction machine based on spiral vector theory. *IEEE Trans. Ind. Appl.* **2016**, *52*, 1380–1389. [CrossRef]
13. Poza, J.; Oyarbide, E.; Sarasola, I.; Rodriguez, M. Vector control design and experimental evaluation for the brushless doubly fed machine. *IET Electr. Power Appl.* **2009**, *3*, 247–256. [CrossRef]
14. Shao, S.; Abdi, E.; Barati, F.; McMahon, R. Stator-flux-oriented vector control for brushless doubly fed induction generator. *IEEE Trans. Ind. Electron.* **2009**, *56*, 4220–4228. [CrossRef]
15. Protsenko, K.; Xu, D. Modeling and control of brushless doubly-fed induction generators in wind energy applications. *IEEE Trans. Power Electron.* **2008**, *23*, 1191–1197. [CrossRef]
16. Basic, D.; Zhu, J.G.; Boardman, G. Transient performance study of a brushless doubly fed twin stator induction generator. *IEEE Trans. Energy Convers.* **2003**, *18*, 400–408. [CrossRef]
17. Shao, S.; Long, T. Dynamic control of the brushless doubly fed induction generator under unbalanced operation. *IEEE Trans. Ind. Electron.* **2013**, *60*, 2465–2476. [CrossRef]
18. Chen, J.; Zhang, W.; Chen, B.; Ma, Y. Improved vector control of brushless doubly fed induction generator under unbalanced grid conditions for offshore wind power generation. *IEEE Trans. Energy Convers.* **2016**, *31*, 293–303. [CrossRef]
19. Xu, L.; Cheng, M.; Wei, X.; Yan, X.; Zeng, Y. Dual synchronous rotating frame current control of brushless doubly fed induction generator under unbalanced network. *IEEE Trans. Ind. Electron.* **2021**, *36*, 6712–6724. [CrossRef]
20. Taufik, T.; Leposava, R.; Milutin, J. Dynamic Modeling and Control of BDFRG under Unbalanced Grid Conditions. *Energies* **2021**, *14*, 4297. [CrossRef]
21. Cai, D.; Liu, H.; Hu, S.; Sun, G.; Wang, E.; Tang, J. A Proportional-Integral-Resonant Current Control Strategy for a Wind-Driven Brushless Doubly Fed Generator during Network Unbalance. *Electronics* **2024**, *13*, 1616. [CrossRef]
22. Hu, S.; Zhu, G. Enhanced control and operation for brushless doubly-fed induction generator basedwind turbine system under grid voltage unbalance. *Electr. Power Syst. Res.* **2022**, *207*, 117861. [CrossRef]
23. Hu, S.; Zhu, G.; Kang, Y. Modeling and coordinated control design for brushless doubly-fed induction generator based wind turbine to withstand grid voltage unbalance. *IEEE Access* **2021**, *36*, 63331–63344. [CrossRef]
24. Cai, D.; Chen, R.; Hu, S.; Sun, G.; Wang, E.; Tang, J. An Improved Collaborative Control Scheme to Resist Grid Voltage Unbalance for BDFG-BasedWind Turbine. *Electronics* **2024**, *13*, 3582. [CrossRef]
25. Voltolini, H.; Carlson, R. Grid synchronization and maximum power point tracking for wind energy generation system with brushless doubly fed induction generator. In Proceedings of the 34th Annual Conference of IEEE Industrial Electronics, Orlando, FL, USA, 10–13 November 2008; pp. 2173–2177.
26. Xue, X.; Huang, J.; Sang, S. Innovative Inertial Response Imitation and Rotor Speed Recovery Control Scheme for a DFIG. *Electronics* **2023**, *12*, 1029. [CrossRef]
27. Chakraborty, A.; Maity, T. A novel application of adaptive filtering algorithm for LVRT capability enhancement of grid-connected DFIG-based wind energy conversion systems (WECS). *Electr. Power Syst. Res.* **2023**, *217*, 109179. [CrossRef]
28. Zeng, Y.; Cheng, M.; Wei, X.; Xu, L. Dynamic modeling and performance analysis with iron saturation for dual-stator brushless doubly fed induction generator. *IEEE Trans. Energy Convers.* **2020**, *35*, 260–270. [CrossRef]

Disclaimer/Publisher's Note: The statements, opinions and data contained in all publications are solely those of the individual author(s) and contributor(s) and not of MDPI and/or the editor(s). MDPI and/or the editor(s) disclaim responsibility for any injury to people or property resulting from any ideas, methods, instructions or products referred to in the content.